Dalton Transactions

Accepted Manuscript

ROYAL SOCIETY OF CHEMISTRY

www.rsc.org/dalton

Crystal structure evolution and luminescence properties of color tunable solid solution phosphors $Ca_{2+x}La_{8-x}(SiO_4)_{6-x}(PO_4)_xO_2:Eu^{2+}$

Yufei Xia[†], Jian Chen[†], Yan-gai Liu*[, †], Maxim S. Molokeev[§, ♣], Ming Guan[†], Zhaohui Huang[†], Minghao Fang[†]

[†] *School of Materials Science and Technology, Beijing Key Laboratory of Materials Utilization of Nonmetallic Minerals and Solid Wastes, National Laboratory of Mineral Materials, China University of Geosciences, Beijing, 100083*

§Laboratory of Crystal Physics, Kirensky Institute of Physics, SB RAS, Krasnoyarsk 660036, Russia

♣ Department of Physics, Far Eastern State Transport University, Khabarovsk 680021, Russia

[*] Corresponding author:

* Yan-gai Liu, Email: liuyang@cugb.edu.cn

Abstract:

A series of apatite solid solution phosphors $Ca_{2+x}La_{8-x}(SiO_4)_{6-x}(PO_4)_xO_2:Eu^{2+}$ (x=0,2,4,6) were synthesized by conventional high-temperature solid-state reaction. The phase purity was examined by XRD, XPS and XRF. The crystal structure information, such as the concentration, cell parameters and occupation rate, were analyzed by Rietveld refinement, demonstrating that the Eu^{2+} activated $Ca_2La_8(SiO_4)_6O_2$ and $Ca_8La_2(PO_4)_6O_2$ to form a continuous solid solution phosphors. The different behaviors of luminescence evolution in response to structural variation were verified among the series of phosphors. The two kinds of Eu^{2+} ion sites were proved by low temperature PL spectra (8k) and room temperature decay curves, and the substitution of large

La^{3+} ion by small Ca^{2+} ion induced the decreased crystal field splitting of Eu^{2+} ion, which caused the increase in emission energy from the 5d excited state to the 4f ground state and a resultant blue-shift from 508nm to 460nm. Therefore, with the crystal structure evolution, the emitting color of the series phosphors can be controlled from green to blue by adjusting the ratio of Ca/La.

Key Words: luminescence, apatite phosphors, solid solution, crystal structure variation

1. Introduction

Compared to the conventional incandescent or fluorescent lamps, the LED-based lighting device fabricated by coating the yellow-emitting phosphor YAG: Ce^{3+} on blue InGaN LED chip has aroused a revolution in lamp industry due to many advantages, such as significant power reduction, longer lifetime, higher luminous efficiency, environmental friendliness and brightness.[1-3] However, this combination exhibits poor color rendering index (CRI ≈ 70-80) and high correlated color temperature (CCT ≈ 7750 K) attributes to the insufficient red emission.[4, 5] One solution is to assemble LEDs by pumping a near-ultraviolet (n-UV) emitting chip with a mixture of blue, green and red emitting phosphors,

which can obtain high quality white light with the smoother spectral distribution over the whole visible range.[6, 7]

As the most frequently used activator in phosphors, the crystal field strength and coordination environment have great influences on the outermost electron transition of Eu^{2+} ion because the active electronic level is not shielded against the surrounding ligands,[8-10] indicating that Eu^{2+} ion can emit various lights from the ultraviolet to the infrared with broadband emitting fluorescence.[11, 12] As well known that the apatite structure compounds (space group $P6_3/m$), with a general chemical formula of the form $A_{10}(XO_4)_6Z_2$ (A = Ca^{2+},Ba^{2+},Ce^{3+},La^{3+},Y^{3+}, etc., X = P^{5+},As^{5+},Si^{4+}, etc., and Z =O^{2-},F^-,Cl^-,OH^-, etc.),[13] contains two kinds of cations sites: the 9-fold coordinated 4f sites with C_3 point symmetry and 7-fold coordinated 6h sites with C_S point symmetry, which are suitable for the substitution of various rare-earth-metal ions.[14-16] In consequence, due to the adjustable structures, excellent thermal and physicochemical stability, apatite compounds have become highly efficient host materials for the luminescence of various rare earth ions and aroused wide attention.[17-19] As discussed above, the coordination environment of Eu^{2+} site is anticipated to be changed via chemical composition variation among solid solution phosphors.[20] Thus, the emitting color can be controlled by doping Eu^{2+} ion in a series of apatite solid solution hosts which are expected to display adjustable emission spectrum in wide range

to meet the requirements of multi-color phosphors.

In this study, owing to the coordination environment variation of Eu^{2+} ion has been realized by the replacement of Ca^{2+} to La^{3+} ion and result in the crystal splitting decreases of Eu^{2+} ion, a series of color tunable solid solution phosphors $Ca_{2+x}La_{8-x}(SiO_4)_{6-x}(PO_4)_xO_2:Eu^{2+}$ (x=0,2,4,6) were successfully prepared by high-temperature solid-state reaction. Moreover, it's worth noting that the replacement of $[PO_4]^{3-}$ to $[SiO4]^{4-}$ tetrahedron was introduced into the solid solution to realize charge compensation because of the different valence between Ca^{2+} - La^{3+} and that the $Ca_4La_6(SiO_4)_4(PO_4)_2O_2:Eu^{2+}$ and $Ca_6La_4(SiO_4)_2(PO_4)_4O_2:Eu^{2+}$ phosphors were synthesized on first time.

The phase purity was demonstrated by XRD, XPS and XRF, and the crystal structure information was analyzed base on Rietveld refinement results. On the other hand, the relationship between crystal structure evolutions, the PLE and PL spectra at normal and low temperature, lifetimes and temperature dependence spectra have been discussed in detail.

2. Experimental

2.1. Materials and synthesis

A series of apatite solid solution phosphors $Ca_{2+x}La_{8-x}(SiO_4)_{6-x}(PO_4)_xO_2$:0.02$Eu^{2+}$ (x=0,2,4,6) were synthesized according to the conventional high-temperature solid-state method. Ca_2CO_3 (analytical reagent (A. R.)), La_2O_3 (A. R.), SiO_2 (A. R.), $NH_4H_2PO_4$ (A. R.), and Eu_2O_3 (A. R.) were used as raw materials. After raw materials were well ground in agate mortar for 10 min according the stoichiometric amounts of reactants, all the materials were preheated for 1 h at 1000 °C in corundum crucible to eliminate H_2O and CO_2. Then, the mixed powders were sintered at 1525 °C in a reductive atmosphere (H_2 10%, N_2 90%) for 6 h in a horizontal tube furnace. Finally, the sintered products were well ground after cooling down to room temperature.

2.2. Characterization

The X-ray diffraction (XRD) data of powder samples were collected on an X-ray powder diffractometer (D/max-IIIA, Rigaku, Japan) with a step-wise scanning mode over the 2θ range of 10°–110° by using Cu Kα radiation (1.5406 Å) under the operating voltage (40 kV) and current (100 mA). The XRD patterns, which were submitted for Rietveld refinement, were acquired in the step size of 0.02° and counting time of 2 s per step.

X-ray photoelectron spectroscopy (XPS) measurements were collected

with Kratos Axis Ultra DLD, employing MCP stack & delay-line photoelectron detector with scanned & snapshot spectroscopy modes. X-ray Fluorescence (XRF) measurements were measured by utilizing a Rigaku ZSX Primus II X-ray fluorescence spectrograph. The photoluminescence emission (PL) spectrum and the photoluminescence excitation (PLE) spectrum at 298k and 8k were measured by using a Hitachi F-4600 fluorescence spectrophotometer (Japan) equipped with a 150-W Xe lamp as the excitation source. The temperature-dependent luminescence properties were measured on the same spectrophotometer which was assembled with a computer-controlled electric furnace and a self-made heating attachment. The morphology was observed using high-resolution transmission electron microscopy (HRTEM; JEM-21000, JEOL, Japan). The room-temperature luminescence decay curves were obtained from a spectrofluorometer (Horiba, Jobin Yvon TBXPS) using a tunable pulse laser radiation (nano-LED) as the excitation.

3. Results and Discussion

3.1. Phase formation and structural characteristics

The XRD patterns of $Ca_{2+x}La_{8-x}(SiO_4)_{6-x}(PO_4)_xO_2$:0.02$Eu^{2+}$ (x=0,2,4,6) and the standard PDF card (JCPDF 29-0337) of $Ca_2La_8(SiO_4)_6O_2$ were displayed in Fig. 1a. All the diffraction peaks of these samples matched well with the JCPDF 29-0337 card, indicating that the series of solid

solution phosphors have been prepared successfully and that the introduction of Eu^{2+} ion did not cause any impurity phase. In addition, the diffraction peaks of the last three samples (x=2, 4, 6) have obviously shift towards the high degree with the increase of the ratio of Ca/La. It can be explained that the substitution of large La^{3+} ion by small Ca^{2+} ion and large $[SiO4]^{4-}$ tetrahedron by small $[PO4]^{3-}$ tetrahedron causes an decrease in the lattice constant of $Ca_{2+x}La_{8-x}(SiO_4)_{6-x}(PO_4)_xO_2$ hosts,[21] which is also an evidence demonstrating the existence of solid solution in the whole range (x=0,2,4,6).[9] Photoelectron survey spectra of the $Ca_6La_4(SiO_4)_2(PO_4)_4O_2$:0.02$Eu^{2+}$ sample is plotted in Fig.1b, depicting photoelectron peaks corresponding to O 2s, Si 2p, P 2p, La $4p_{3/2}$, Ca 2p, Ca 2s, O 1s, La $3d_{5/2}$, La $3d_{3/2}$ and Eu $3d_{5/2}$ emission. The insert shows high-resolution XPS spectra at Eu $3d_{5/2}$ position, and the peak at 1126.28ev is agree well with the signal of Eu^{2+} $3d_{5/2}$, demonstrating the existence of Eu^{2+} ion. Furthermore, elements contents of $Ca_6La_4(SiO_4)_2(PO_4)_4O_2$:0.02$Eu^{2+}$ sample was further examined and calculated by XRF. As shown in Table 1, the proportions of all components are matching well with the suggestion formula.

Table 1. The main parameters of XRF measurement

Component	Result	Unit	Intensity	Spectral lines of elements
O	23.5	mass%	0.0745	O-KA
Si	3.17	mass%	3.064	Si-KA
P	8.04	mass%	20.233	P-KA
Ca	18.7	mass%	35.581	Ca-KA
La	42.5	mass%	6.245	La-LA
Eu	1.55	mass%	0.5759	Eu-LA

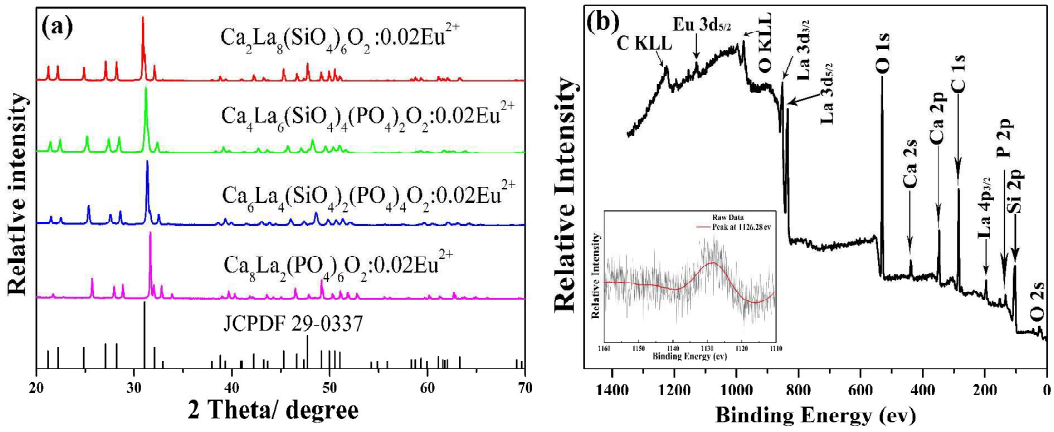

Fig. 1. (a) The XRD patterns of $Ca_{2+x}La_{8-x}(SiO_4)_{6-x}(PO_4)_xO_2$:0.02$Eu^{2+}$ (x=0,2,4,6) and the standard PDF card (JCPDF 29-0337) of $Ca_2La_8(SiO_4)_6O_2$. (b) The photoelectron survey spectra of the $Ca_6La_4(SiO_4)_2(PO_4)_4O_2$:0.02$Eu^{2+}$ sample.

Fig. 2a displays the crystal structure of 2×2×2 unit cells of $Ca_4La_6(SiO_4)_4(PO_4)_2O_2$, which is chosen as the representative. Obviously, $Ca_4La_6(SiO_4)_4(PO_4)_2O_2$ has layered structure and contains two kinds of cation sites: the inner-laminar site labeled M(I) with the local symmetry C_3 and the inter-laminar site labeled M(II) with the local symmetry C_s.[22]

The two kinds of different coordination environments of cation sites were displayed in Figs. 2b and 2c, respectively. The M(I) site at the 4f site (C_3) was surrounded by 9 oxygen atoms to form a mono-caped square antiprism, which was connected with tetrahedral PO_4/SiO_4 groups, and the M(II) site at the 6h site (C_S) formed pentagonal bipyramid with the surrounding 7 oxygen atoms and these bipyramid were connected with each other through vertex. Theoretically, both of the Ca^{2+} ion and La^{3+} ion are uniformly distributed in the two kinds of cationic sites,[23] illustrating that the ratio of Ca/La is easily changed by adjusting the proportion of raw materials.

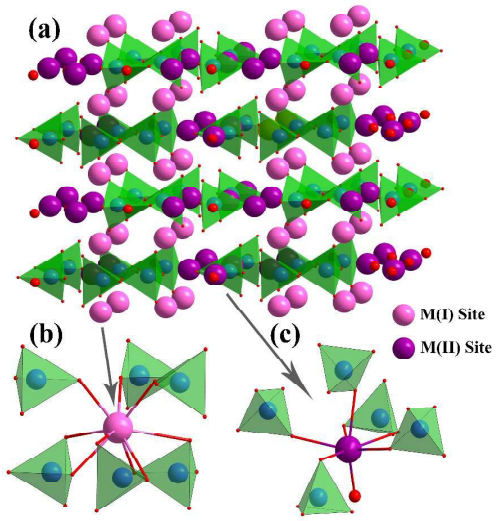

Fig. 2. (a) The crystal structure of 2×2×2 unit cells of $Ca_4La_6(SiO_4)_4(PO_4)_2$:0.02$Eu^{2+}$, (b) The coordination environment of M(I) site with the local symmetry C_3 and (c) the M(II) site with the local symmetry C_S.

Table 2. The main refinement parameters of $Ca_{2+x}La_{8-x}(SiO_4)_{6-x}(PO_4)_xO_2$ (x=0, 2, 4, 6).

Compound	$x = 0$	$x = 2$	$x = 4$	$x = 6$
Sp.Gr.	$P6_3/m$	$P6_3/m$	$P6_3/m$	$P6_3/m$
a, Å	9.6559(1)	9.5948(6)	9.5325(4)	9.4606(2)
b, Å	9.6559(1)	9.5948(6)	9.5325(4)	9.4606(2)
c, Å	7.1529(1)	7.0882(5)	7.0206(4)	6.9356(1)
α, ^{O}	90	90	90	90
β, ^{O}	90	90	90	90
γ, ^{O}	120	120	120	120
V, Å^3	577.56(2)	565.12(8)	552.49(6)	537.59(2)
2θ-interval,	10-110	10-110	10-110	10-110
$R_{wp,}$ %	10.038	11.012	10.135	10.065
$R_{exp,}$ %	1.311	1.299	1.287	1.325
$R_{B,}$ %	2.268	2.168	1.792	2.777

The four XRD patterns were analyzed by Rietveld refinement. The observed (×), calculated (red) and difference (gray) XRD profiles for the refinement of $Ca_{2+x}La_{8-x}(SiO_4)_{6-x}(PO_4)_xO_2$ (x=0,2,4,6) were shown in Figs. 3a-3d. The main refinement parameters of processing and refinement results were presented in Table 2. The results of refinement further demonstrate that the series solid solution phosphors are single phase without any impurity or secondary phase. On the other hand, the ranges of the weighted profile R-factor (R_{wp}) and R-Bragg factor (R_B) are

10.038%-11.012% and 1.792%-2.777%, respectively, indicating that the crystal structure of these phosphors matches well with the starting model ($Ca_2La_8(SiO_4)_6$) after refinement and that the results are believable and publishable. Meanwhile, we also refined the concentration of these samples while obtaining the high-quality XRD data. According to the refinement results, the calculated formula are respectively $Ca_{2.87(2)}La_{7.13(2)}(SiO_4)_6O_2$, $Ca_{4.47(2)}La_{5.53(2)}(SiO_4)_{3.53(2)}(PO_4)_{2.47(2)}O_2$, $Ca_{5.52(2)}La_{3.48(2)}(SiO_4)_{1.48(2)}(PO_4)_{4.52(2)}O_2$ and $Ca_{8.28(2)}La_{1.72(2)}(PO_4)_6O_2$, demonstrating that the actually refined concentrations are well consistent with the suggested formula and that the coordination environment variation is mainly caused by the replacement of Ca^{2+} to La^{3+} ion. Moreover, according to the XRD data and the Rietveld refinement, no additive superstructure peaks were detected, these features prove that Ca^{2+} ion and La^{3+} ion were randomly mixed at the atomic level.[24] In addition, the unit lattice parameters and unit cell volume of the as-prepared phosphors were given in Fig. 4. The high linear fitting coefficients (0.99334-0.99796) proved the crystal structure evolution of this continuous solid solution. The lattice parameters and unit cell volume show linear decrease and are proportional to the value of *x*, which is attribute to the substitution of large La^{3+} ion by small Ca^{2+} ion, suggesting that the coordination environment of cations become more unconsolidated with the x increases.[25]

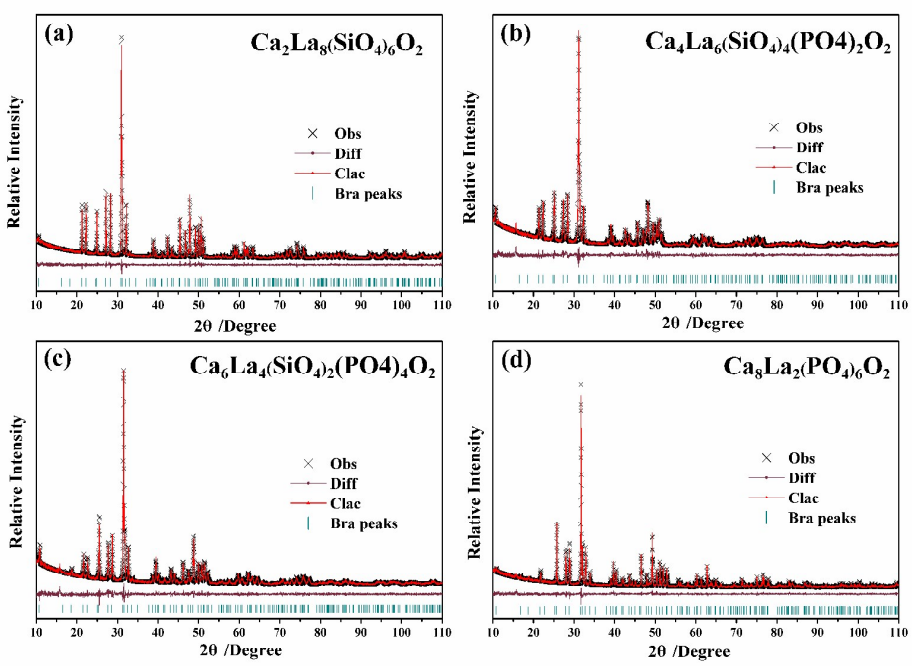

Fig. 3a-d. Powder XRD pattern (×) of $Ca_{2+x}La_{8-x}(SiO_4)_{6-x}(PO_4)_xO_2$:0.02$Eu^{2+}$ (x=0,2,4,6) samples with corresponding Rietveld refinement (red) and residuals (gray).

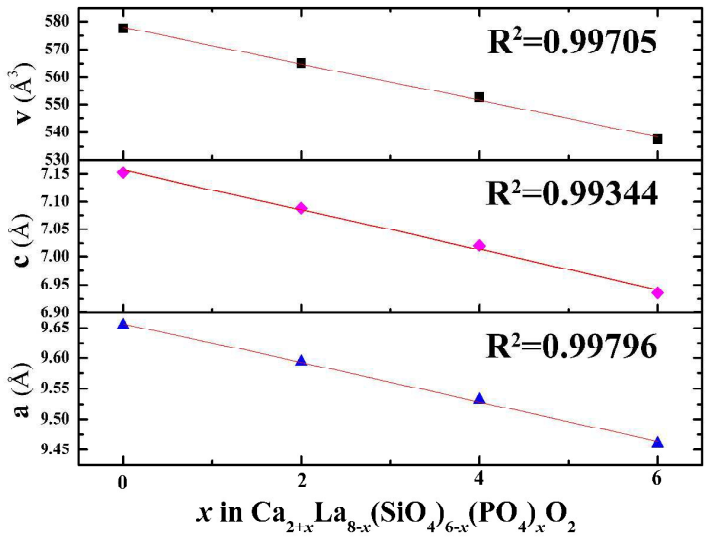

Fig. 4. The refined unit cell parameters (a, c) and cell volume of $Ca_{2+x}La_{8-x}(SiO_4)_{6-x}(PO_4)_xO_2$:0.02$Eu^{2+}$ (x=0,2,4,6).

As shown in Figs. 5a-5d, the linear change crystal structure of these solid solution phosphors were further verified by HRTEM and fast Fourier transform (FFT) images. Both HRTEM and FFT images illustrate that no significant structural defect appeared in the selected area of these single-phase samples and that the good crystallinity was obtained. Moreover, the lattice fringes measurements with the *d* spacing of 0.315 nm, 0.837 nm, 0.354 nm, and 0.353 nm could be assigned to the planes (210), (010), (021) and (021) for $Ca_{2+x}La_{8-x}(SiO_4)_{6-x}(PO_4)_xO_2:0.02Eu^{2+}$ (x=0,2,4,6), respectively. The measured *d* spacing in different orientations could be transformed into the same *d* spacing value of (021) according to the classic Bragg equation.[24] Therefore, the normalized *d* spacing of (021) were calculated to be 0.358 nm, 0.356 nm, 0.354 nm and 0.353 nm, respectively. Consequently, the decrease of *d* spacing is well consistent with the refinement results, indicating the existence of structural evolution in the series of solid solution.

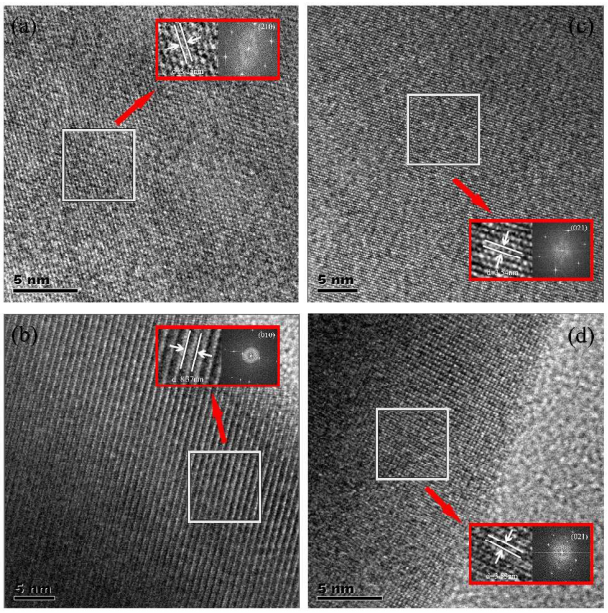

Fig. 5. HRTEM and FFT images for $Ca_{2+x}La_{8-x}(SiO_4)_{6-x}(PO_4)_xO_2$:0.02$Eu^{2+}$ with different x values, x=0 (a), x=2 (b), x=4 (c) and x=6 (d).

Table 3. Atomic occupation rates in $Ca_{2+x}La_{8-x}(SiO_4)_{6-x}(PO_4)_xO_2$ with different x values.

Sites	$x = 0$	$x = 2$	$x = 4$	$x = 6$
Ca1	0.12(2)	0.20(2)	0.43(1)	0.714(7)
La1	0.88(2)	0.80(2)	0.57(1)	0.286(7)
Ca2	0.53(1)	0.81(1)	0.983(7)	1.000(6)
La2	0.47(1)	0.19(1)	0.017(7)	0.000(6)

The effective ionic radii of Ca^{2+} ion are 1.18 (CN=9) and 1.06 Å (CN=7) and the effective ionic radii of La^{3+} ion are 1.21 (CN=9) and 1.10 Å (CN=7). Theoretically, considering the similar ion radius and valence, Eu^{2+} ion ($R_{CN=9}$=1.3, $R_{CN=7}$=1.2) is expected to substitute the La^{3+} and Ca^{2+} sites in the $Ca_{2+x}La_{8-x}(SiO_4)_{6-x}(PO_4)_xO_2$ (x=0,2,4,6) crystal structure.[26] Therefore, four kinds of emitting blocks will be included in the host: Ca(I), Ca(II), La(I) and La(II). The occupation rates of Ca(I), Ca(II), La(I), and La(II), reflecting the distribution of Ca^{2+} ion and La^{3+} ion in the two cationic sites, have been refined and displayed in Table 3. When the content of Ca^{2+} ion is increase, the occupation rate of La(II) is decreased faster than that of La(I) and the M(II) site is totally occupied by Ca^{2+} ion while the chemistry formula is $Ca_8La_2(PO_4)_6O_2$ (x=6), which shows similar results with the previous studies.[16, 26] The phenomenon can be explained as follows: the Eu^{2+} ion located at M(II) site that connected with a free oxygen ion, resulting a very short Eu-O distance due to the small sum of the electrostatic bond strength of the cations toward free oxygen ion. Thus, it must be very unfavorable for the (6 h) sites occupied by cation with large radius in these compounds.[27]

3.2. Photoluminescence Characteristics

The PLE spectra (monitored at the range of 460nm-508nm) and the PL spectra (under 365nm excitation) of $Ca_{2+x}La_{8-x}(SiO_4)_{6-x}(PO_4)_xO_2$:0.02$Eu^{2+}$ (x=0,2,4,6) phosphors at room temperature were displayed in Figs. 6a-6b,

respectively. The PLE spectra depict a series of broad excitation bands between 250nm and 450nm, which are attributed to the $4f^7 \rightarrow 4f^6 5d^1$ transition of the Eu^{2+} ion,[28] and the emission spectra show a series of broad emission bands from 400nm to 650nm, which are attributed to the 5d → 4f transition of the Eu^{2+} ion. As shown in Fig. 6b, a strong asymmetric broad band with a maximum wavelength peaked at 508nm was detected in the PL spectrum of $Ca_2La_8(SiO_4)_6O_2:0.02Eu^{2+}$, which was chosen as the representative of the solid solution phosphors. The asymmetric emission band can be well decomposed into two Gaussian components peaked at 504nm (I1) and 542nm (I2), respectively, demonstrating the existence of two types of emitting centers in $Ca_2La_8(SiO_4)_6O_2:0.02Eu^{2+}$.

Fig. 6c-6d display the low temperature (8k) PLE and PL spectra of $Ca_2La_8(SiO_4)_6O_2:0.02Eu^{2+}$ and $Ca_8La_2(PO_4)_6O_2:0.02Eu^{2+}$. The PL spectra of $Ca_2La_8(SiO_4)_6O_2:0.02Eu^{2+}$ can be well separated into two components peaked at 526nm and 576nm, and the PL spectra of $Ca_8La_2(PO_4)_6O_2:0.02Eu^{2+}$ obviously contains two components peaked at 460nm and 625nm, respectively. The results further demonstrate that there are two kinds of cation sites included in the series apatite phosphors which could be occupied by Eu^{2+} ion.

Actually, considering the valence state and previous results,[16, 29] the blue emission band observed in the PL spectrum of

$Ca_2La_8(PO_4)_6O_2$:0.02Eu^{2+} is attributed to the substitution of Ca^{2+} ion by Eu^{2+} ion. According to the report by Van Uitert, to further demonstrate the relationship between emission peaks and emission centers, the possible crystallographic site may be investigated theoretically by the following equation:[30]

$$E(cm^{-1}) = Q^*\left[1-\left(\frac{V}{4}\right)^{1/V}\times 10^{-(nEar)/80}\right], \quad (1)$$

where E represents the position of the d-band edge in energy for the rare-earth ion (cm^{-1}); Q^* is the energy position for the lower d-band edge for the free ion (34000 cm^{-1} for Eu^{2+}); V is the valence of the activator (Eu^{2+}) ion (V = 2); n is the number of anions in the immediate shell around the Eu^{2+} ion; r is the radius of the host cationic replaced by the Eu^{2+} ion (in Å); Ea is the electron affinity of the atoms that form anions (in eV) depending on the anion complex type. Here, Ea was approximately determined as 1.60 for the $[SiO_4]^{4-}$ in oxide host[31] and r values of Ca (I) and Ca (II) were calculated to be 118 pm and 106 pm, respectively. Consequently, the E_{calcd} values of Ca (I) and Ca (II) were calculated to be 19693 cm^{-1} and 18546 cm^{-1}, respectively. The result indicated that the emission band centered at 504nm was attributed to Eu^{2+} ion occupying the Ca(I) site with C_3 symmetry and nine-coordination and that the emission band peaked at 542nm was attributed to the Eu^{2+} ion occupying the Ca(II) site with C_S symmetry and seven-coordination.

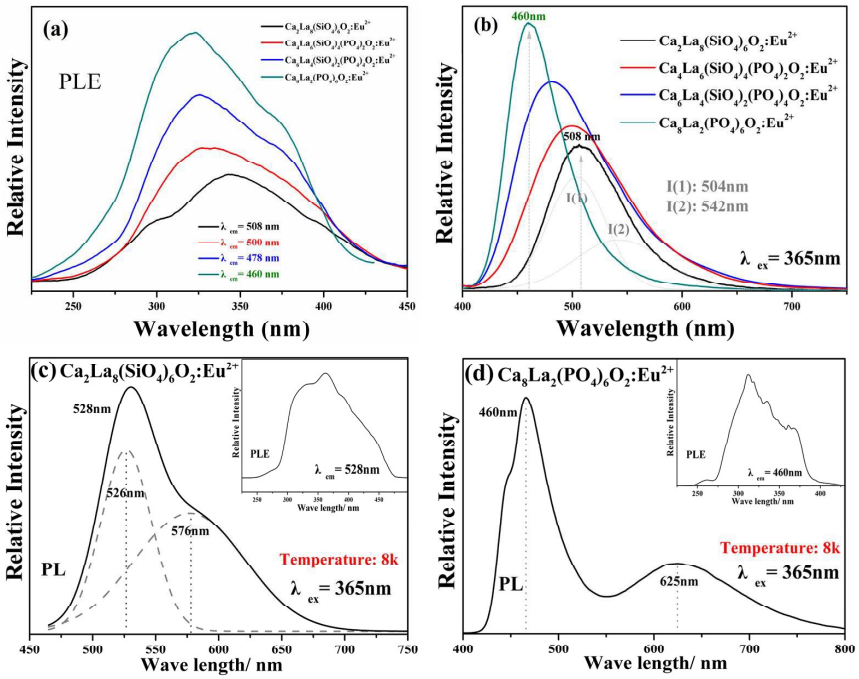

Figs.6a-6d. (a) The PLE monitored at the range of 460nm-508nm and (b) the PL spectra under 365nm excitation of $Ca_{2+x}La_{8-x}(SiO_4)_{6-x}(PO_4)_xO_2$:0.02$Eu^{2+}$ (x=0,2,4,6) at room temperature. (c) The PL and PLE spectra at low temperature (8k) of $Ca_2La_8(SiO_4)_6O_2$:0.02Eu^{2+} and (d) the PL and PLE spectra at low temperature (8k) of $Ca_8La_2(PO_4)_6O_2$:0.02Eu^{2+}

The emission wavelength of the $Ca_{2+x}La_{8-x}(SiO_4)_{6-x}(PO_4)_xO_2$:0.02$Eu^{2+}$ (x=0,2,4,6) PL spectra shows a wide blue shift from 508nm to 460nm with the increase of x value which is depend on the crystal field strength variation. The structural model of cation substitution around Eu^{2+} ion sites were depicted in Fig. 7. In this regards, the crystal field splitting of Eu^{2+} ion can be determined as obeying:[17, 32, 33]

$$Dq = \frac{ze^2r^4}{6R^5} \qquad (2)$$

Where Dq is a measure of energy level separation, R represents the

distance from the central ion to its ligands, *z* stand for the charge or valence of the anion, *r* is the radius of the d wave function, and *e* is the charge of an electron. For the $d_{(Eu–O)}$-orbital, if *z*, *e* and *r* are equal, then *Dq* is only the function of $1/R^5$. When the large La^{3+} ion substituted by small Ca^{2+} ion, the distance between Eu^{2+} and O^{2+} becomes longer and the magnitude of the crystal field strength decreases.[34, 35] Thus, the crystal field splitting of Eu^{2+} ion is reasonable decrease and results in a gradually increase of the lowest 5d state.[36] As a consequence, the emission wavelength shows a blue shift among the as-prepared phosphors and color variation from green to blue.

Table 3. Excitation and Emission Bands, Stokes Shift, Crystal Field Splitting of $Ca_{2+x}La_{8-x}(SiO_4)_{6-x}(PO_4)_xO_2:0.02Eu^{2+}$ (*x*=0,2,4,6) phosphors.

x values	λ_{ex} range (nm)	FWHM of λ_{ex} (nm)	λ_{em} (nm)	Stokes shift (cm^{-1})	Crystal field splitting (cm^{-1})
0	250-450	142	508	6135	22230
2	250-450	127	500	6082	20833
4	250-450	118	478	6039	19231
6	250-400	113	460	5985	18190

In addition, as shown in table 3, the stokes shifts were estimated to be 6135 cm^{-1}-5985 cm^{-1} and the full width at half-maximum (FWHMs) of the PLE spectra decrease from 142nm to 113nm with the increase of *x*. The crystal-field splitting of Eu^{2+} ion were estimated to be

22230cm^{-1}-18190 cm^{-1}, which is calculated by the gap between the first and the last components peak of PLE spectra. All the computation further demonstrate the decrease of crystal field splitting.[37]

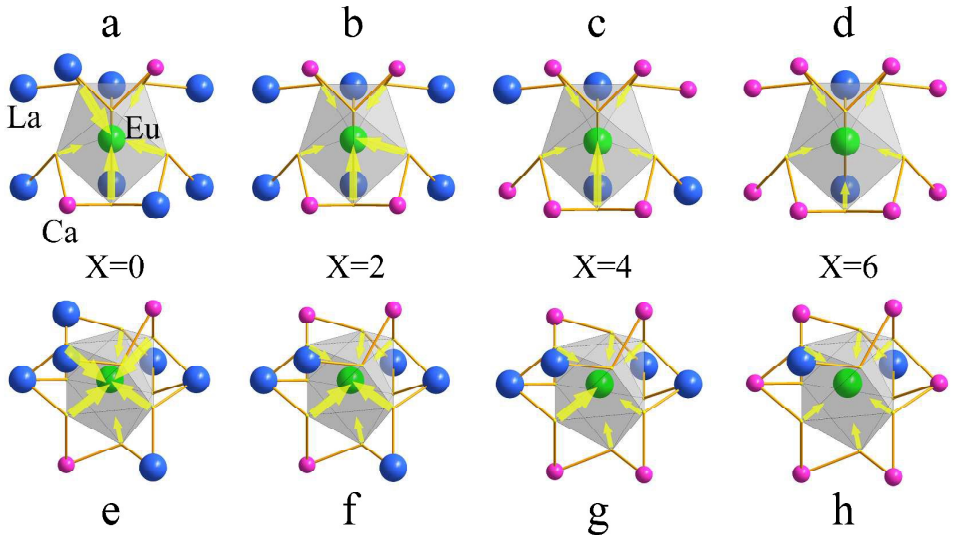

Fig. 7. Structural model for explaining the photoluminescence evolution observed in $Ca_{2+x}La_{8-x}(SiO_4)_{6-x}(PO_4)_xO_2$:0.02$Eu^{2+}$ (x=0,2,4,6) phosphors: (a-d) represent Eu^{2+} located in M(I) site, (e-h) represent Eu^{2+} located in M(II) site.

Furthermore, Fig. 8 presents the room temperature decay curves of Eu^{2+} ion luminescence in $Ca_{2+x}La_{8-x}(SiO_4)_{6-x}(PO_4)_xO_2$:0.02$Eu^{2+}$ (x=0,2,4,6) series. All the decay curves can be well fitted with a second order exponential equation:

$$I(t) = A_1 \exp(-t/\tau_1) + A_2 \exp(-t/\tau_2) \quad (3)$$

Where $I(t)$ is the luminescence intensity, A_1 and A_2 represent constants, τ is the time, τ_1 and τ_2 stand for rapid and slow lifetimes for exponential components, respectively. Moreover, the effective lifetime constant (τ*)

can be calculated as:

$$\tau^* = (A_1\tau_1^2 + A_2\tau_2^2)/(A_1\tau_1 + A_2\tau_2) \quad (4)$$

The effective decay times were calculated to be 745.34, 468.61, 384.15 and 353.33ns with x = 0, 2, 4 and 6, respectively. One can see that the decay times decrease with the increase content of Ca^{2+} ion. Due to the phase structures become more unconsolidated compared to the original $Ca_2La_8(SiO_4)_4$:0.02Eu^{2+} phase, as a consequence, the increasing possibility of energy transfer among Eu^{2+} ion increase the possible non-radiative transition and lead to the decreasing lifetime values.[32, 38] On the other hand, the two decay components (τ_1 and τ_2) also proved the Eu^{2+} occupied two different Ca^{2+} sites.[13]

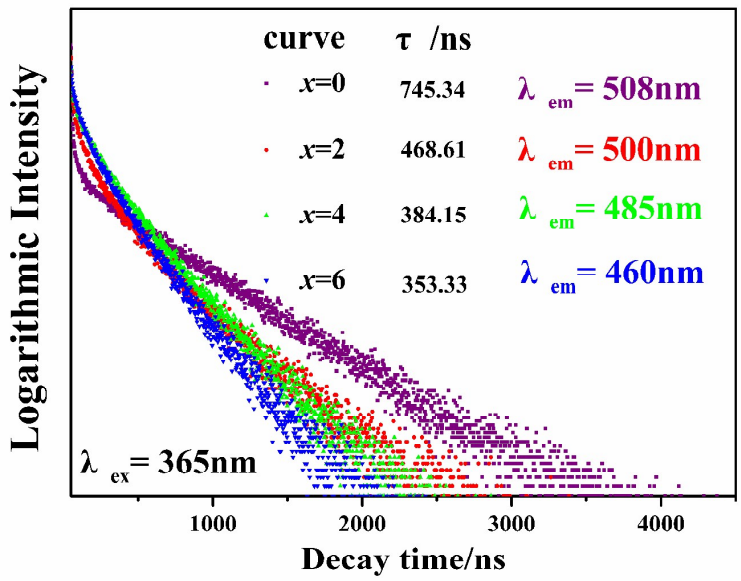

Fig.8 Room temperature decay curves of $Ca_{2+x}La_{8-x}(SiO_4)_{6-x}(PO_4)_xO_2$:0.02$Eu^{2+}$ (x=0,2,4,6) phosphors

The temperature dependence experiment proved that the thermal stability is consistent with the crystal structure evolution in the as-prepared series phosphors, and the peak emission intensity that normalized to 25^{O}C values was depicted in Fig.10. As shown in Fig. 10, the emission intensity of all samples shows a decrease tendency with the increases of temperature. Additionally, the thermal stability gradually decrease with the increasing x values, this phenomenon can be explained by the neighboring-cation effect.[39,40] The replacement of large La^{3+} ion by small Ca^{2+} ion make the distances between the Eu^{2+} activator ion and the neighboring cations become more smaller, as demonstrated by the refined cell parameters and cell volume, resulting in a larger coulombic force following the inverse-square law[41,42] and the decrease of thermal quenching barrier height. Thus, the thermal stability becomes lower with the replacement occurring.

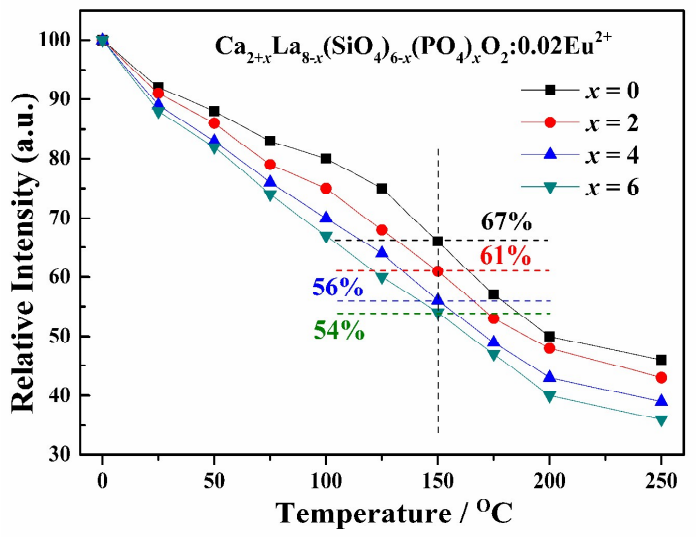

Fig.9. The peak emission intensity of temperature dependence that normalized to 25^{O}C values

Luminescence efficiency is an important technological parameter for phosphors in application. The internal quantum efficiency (QE) of $Ca_{2+x}La_{8-x}(SiO_4)_{6-x}(PO_4)_xO_2$:0.02$Eu^{2+}$ (x=0,2,4,6) phosphors were measured and calculated followed by:[12]

$$\eta_{QE} = \frac{\int L_S}{\int E_R + \int E_S} \quad (5)$$

Where Ls is the luminescence emission spectrum of the sample; E_R represents the spectrum of the excitation light from the empty integrated sphere (without the sample); E_S stand for the excitation spectrum for exciting the sample. As a result, under 365nm excitation, the internal QE of the $Ca_{2+x}La_{8-x}(SiO_4)_{6-x}(PO_4)_xO_2$:0.02$Eu^{2+}$ (x=0,2,4,6) phosphors were estimated to be about 45.44%, 46.39%, 44.12% and 46.56% for x=0,2,4,6, respectively. The QE of the as-prepared phosphors can be further optimized by improve the preparation conditions because the QE depends

closely on the prepared conditions, crystalline defects, particle size and morphology of the phosphor.[25, 39]

The CIE coordinates and the digital photos of $Ca_{2+x}La_{8-x}(SiO_4)_{6-x}(PO_4)_xO_2:0.02Eu^{2+}$ (x=0,2,4,6) phosphors under 365nm excitation are displayed in Fig. 9. The calculated CIE coordinates are (0.2099, 0.4884) for x=0, (0.2167, 0.3585) for x=2, (0.1955, 0.2992) for x=4 and (0.1846, 0.1851) for x=6, respectively. Obviously, both of the digital photos and the coordinates demonstrate that the emitting color of the solid solution phosphors $Ca_{2+x}La_{8-x}(SiO_4)_{6-x}(PO_4)_xO_2:0.02Eu^{2+}$ (x=0,2,4,6) can be adjusted in the wide range from green to blue by changing the ratio of Ca/La.

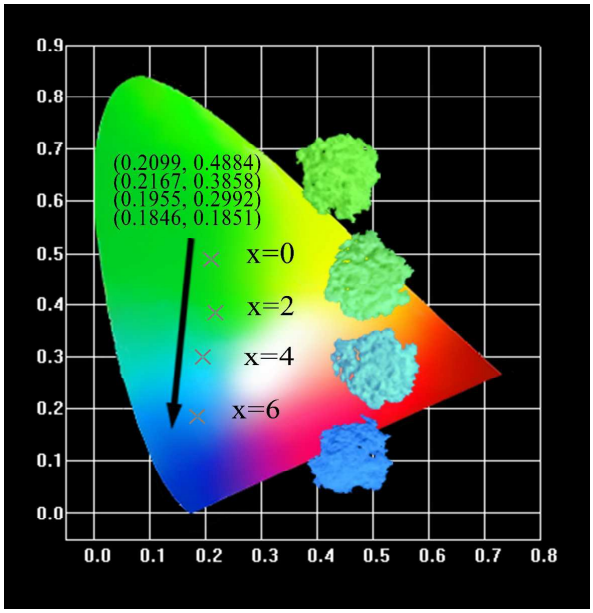

Fig. 10. The CIE coordinates and the digital photos of $Ca_{2+x}La_{8-x}(SiO_4)_{6-x}(PO_4)_xO_2:0.02Eu^{2+}$ (x=0,2,4,6) phosphors.

4. Conclusions

In summary, a series of continuous solid solution phosphors $Ca_{2+x}La_{8-x}(SiO_4)_{6-x}(PO_4)_xO_2$:0.02$Eu^{2+}$ (x=0,2,4,6) were successfully synthesized by the solid-state reaction method. The phase purity was examined by XRD, XPS and XRF, the crystal structure information was identified by Rietveld refinement and HRTEM, respectively. The refined concentration, cell parameters and occupation rate matched well with the suggestion formula and the variation tendency of Ca/La, demonstrating that Eu^{2+} activated $Ca_2La_8(SiO_4)_6O_2$ and $Ca_8La_2(PO_4)_6O_2$ to form a continuous solid solution phosphors. The different behaviors of spectroscopy properties based on structural variation were verified among the series of phosphors. The PL spectra at room temperature and low temperature (8k) were well separated into two components peaks, demonstrating that there are two kinds of Eu^{2+} ion sites included in these apatite phosphors. Furthermore, the short wavelength emission peak is original from Eu^{2+} ion located at 4f site with nine coordination and the long wavelength emission peak is ascribe to Eu^{2+} ion occupied 6h site with seven coordination. Under 365nm excitation, the series phosphors show a strong blue shift from 508nm to 460nm. It can be explained by that the substitution of large La^{3+} ion by small Ca^{2+} ion induced the decreased crystal field splitting of Eu^{2+} ion, which leads the emission

energy from the 5d excited state to the 4f ground state increases. Consequently, the emitting color of the series phosphors can be controlled from green to blue by adjusting the ratio of Ca/La.

Acknowledgment

This work was sponsored by National Natural Science Foundation of China (Grant No.51472223), the Program for New Century Excellent Talents in University of Ministry of Education of China (Grant No. NCET-12-0951) and the Fundamental Research Funds for the Central Universities (Grant No. 2652015020).

References

1. W. R. Liu, C. H. Huang, C. W. Yeh, J. C. Tsai, Y. C. Chiu, Y. T. Yeh and R. S. Liu, *Inorg. Chem.*, 2012, **51**, 9636.
2. H. Wu, X. M. Zhang, C. F. Guo, J. Xu, M. M. Wu and Q. Su, *Photonics Tech. L.*, 2015, **17**, 1160-1162.
3. X. J. Zhang, L. Huang, F. J. Pan, M. M. Wu, J. Wang, Y. Chen and Q. Su, *ACS Appl. Mater. Interfaces*, 2014, **6**, 2709-2717.
4. M. M. Shang, D. L. Geng, D. M. Yang, X. Kang, Y. Zhang and J. Lin, *Inorg. Chem.*, 2013, **52**, 3102-3112.
5. Z. G. Xia, Y. Y. Zhang, M. S. Molokeev and V. V. Atuchin, *J. Phys. Chem. C*, 2013, **117**, 20847-20854.
6. J. Chen, Y. G. Liu, M. H. Fang and Z. H. Huang, *Inorg. Chem.*, 2014, **53**, 11396-11407.
7. X. J. Zhang, J. Wang, L. Huang, F. J. Pan, Y. Chen, B. F. Lei, M. Y. Peng and M. M. Wu, *ACS Appl. Mater. Interfaces*, 2015, **7**, 10044-10054.
8. J. Chen, G. L. Y, H. K. Liu, H. Ding, M. H. Fang and Z. H. Huang, *Opt. Mater.*, 2015, **42**, 80-86.
9. M. Zhang, J.Wang, Z. Zhang, Q. Zhang and Q. Su, *Appl Phys B*, 2008, **93**, 829–835.
10. K. H. Kwon, W. B. Im, H. S. Jang, H. S. Yoo and D. Y. Jeon, *Inorg. Chem.*, 2009, **48**, 11525–11532.
11. P. Dorenbos, *J. Lumin.*, 2003, **104**, 239 - 260.
12. J. Chen, Y. G. Liu, L. F. Mei, H. K. Liu, M. H. Fang and Z. H. Huang, *Sci. Rep.*, 2015, **14**, 13258.
13. Z. Xia, M. S. Molokeev, W. B. Im, S. Unithrattil and Q. Liu, *J. Phys. Chem. C*, 2015, **119**, 9488-9495.
14. G. Zhu, Y. R. Shi, M. Mikami, Y. Shimomura and Y. H. Wang, *Opt. Mater.*, 2013, **3**, 229-236.
15. H. K. Liu, Y. Y. Zhang, L. B. Liao, Q. F. Guo and L. F. Mei, *Ceram. Int.*, 2014, **40**, 13709–13713.
16. M. M. Shang, G. G. Li, D. L. Geng, D. M. Yang, X. J. Kang, Y. Zhang, H. Z. Lian and J. Lin, *J. Phys. Chem. C*, 2012, **116**, 10222−10231.
17. N. Guo, H. P. You, C. Z. Ji, R. Z. Ouyang and D. H. Wu, *Dalton Trans.*, 2014, **43**, 12373-12379.
18. G. G. Li, Y. Zhang, D. L. Geng, M. M. Shang, C. Peng and J. Lin, *ACS Appl. Mater. Interfaces*, 2012, **4**, 296−305.
19. Y. Zhang, G. G. Li, D. L. Geng, M. M. Shang, C. Peng and J. Lin, *Inorg. Chem.*, 2012, **51**, 11655–11664.
20. H. P. Ji, Z. H. Huang, Z. G. Xia, M. S. Molokeev, V. V. Atuchin, M. H. Fang and Y. G. Liu, *J. Phys. Chem. C*, 2015, **119**, 2038−2045.
21. Y. R. Do, K. Y. Ko, S. H. Na and Y. D. Huh, *J. Electrochem. Soc.*, 2006, **153**, 142-146.
22. F. M. Ryan, R. W. Warren, R. H. Hopkins and J. Murphy, *J. Electro chem. Soc.*, 1978, **125**, 1493−1498.

23. W. Y. Huang, F. Yoshimure, K. Ueda, Y. Shimomura, H. S. Sheu, T. S. Chen, H. F. Greer, W. Z. Zhou, S. F. Hu, R. S. Liu and J. P. Attfield, *J. Am. Chem. Soc.*, 2012, **134**, 14108.
24. Z. Xia, Y. Zhang, M. S. Molokeev, V. V. Atuchin and Y. Luo, *Sci. Rep*, 2013, **3**, 3310.
25. K.-W. Huang, W.-T. Chen, C.-I. Chu, S.-F. Hu, H.-S. Sheu, B.-M. Cheng, J.-M. Chen and R.-S. Liu, *Chem. Mater.*, 2012, **24**, 2220-2227.
26. R. E. Ouenzerfia, G. Panczera, C. Goutaudiera, M. T. Cohen-Adada, G. Boulona, M. Trabelsi-Ayedib and N. Kbir-Ariguibc, *Opt. Mater.*, 2001, **16**, 301-310.
27. G. Li, D. Geng, M. Shang, Y. Zhang, C. Peng, Z. Cheng and J. Lin, *J. Phys. Chem. C*, 2011, **115**, 21882–21892.
28. G. Blasse, W. L. Wanmaker, J. W. Tervrugt and A. Bril, *Philips Res. Rep.*, 1968, **23**, 189-200.
29. B. Lee, S. Lee, H. G. Jeong and K. S. Sohn, *ACS Comb. Sci.*, 2011, **13**, 154−158.
30. V. Uitert, *J. Lumin.*, 1984, **29**, 1-9.
31. H. P. Ji, Z. H. Huang, Z. G. Xia, M. S. Molokeev, X. X. Jiang, Z. H. Lin and V. V. Atuchin, *Dalton Trans.*, 2015, **44**, 7679-7686.
32. C. Zhao, Z. Xia and S. Yu, *J. Mater. Chem. C*, 2014, **2**, 6032.
33. C.-H. Huang, P.-J. Wu, J.-F. Lee and T.-M. Chen, *J. Mater. Chem.*, 2011, **21**, 10489.
34. P. Dorenbos, *Phys. Rev. B*, 2001, **64**, 117-125.
35. K. A. Denault, J. Brgoch, M. W. Gaultois, A. Mikhailovsky, R. Petry, H. Winkler, S. P. DenBaars and R. Seshadri, *Chem. Mater.*, 2014, **26**, 2275−2282.
36. C. H. Huang, Y. C. Chiu, Y. T. Ye, T. S. Chan and T. M. Chen, *ACS Appl. Mater. Interfaces*, 2012, **4**, 6661-6668.
37. G. P. Dong, X. D. Xiao, L. L. Zhang, Z. J. Ma, X. Bao, M. Y. Peng, Q. Y. Zhang and J. R. Qiu, *J. Mater. Chem.*, 2011, **21**, 2194-2203.
38. J. Zhou, Z. Xia, M. Chen, M. S. Molokeev and Q. Liu, *Sci. Rep*, 2015, **5**, 12149.
39. N. Guo, Y. Zheng, Y. Jia, H. Qiao and H. You, *J. Phys. Chem. C*, 2012, **116**, 1329–1334.
40. W. Y. Huang, F. Yoshimure, K. Ueda, Y. Shimomura, H. S. Sheu, T. S. Chen, H. F. Greer, W. Z. Zhou, S. F. Hu, R. S. Liu and J. P. Attfield, *J. Am. Chem. Soc.*, 2012, **134**, 14108.
41. D. J. Griffiths, Introduction to Electrodynamics, Prentice Hall, 3rd edn, 1998, ISBN 0-13-805326-X.
42. Z.Y. Wang, Z.G. Xia, M. S. Molokeev, V. V. Atuchin and Q.L. Liu, *Dalton Trans.*, 2014, **43**, 16800.

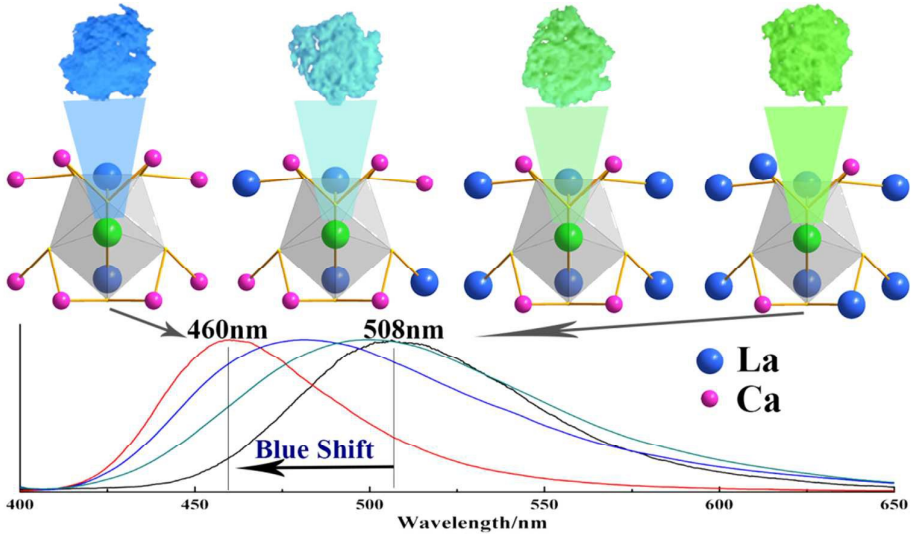

The substitution of La^{3+} by Ca^{2+} lead to crystal structure variation and emitting color changing from green to blue.